J Electroceram (2009) 23:367–371
DOI 10.1007/s10832-008-9469-3

Self-constrained sintering of Al_2O_3/glass/Al_2O_3 ceramics by glass infiltration

Jung-Hun You · Dong-Hun Yeo · Hyo-Soon Shin · Jong-Hee Kim · Ho-Gyu Yoon

Received: 30 May 2007 / Accepted: 7 March 2008 / Published online: 15 April 2008
© Springer Science + Business Media, LLC 2008

Abstract Though need for precise alignment of interlayer patterning in LTCC application, there have been few reports about zero-shrinkage sintering techniques. In this study, ceramic substrate with minimal *x*–*y* shrinkage was prepared by glass infiltration method with 'Al_2O_3/glass/Al_2O_3' structure. Glass infiltration into alumina particle layer was observed with variation of both sintering temperature ($700 \leq T_{sint.} \leq 900$ °C) and alumina particle size distribution ($0.5 \leq D_{50} \leq 1.8$ μm). Since glass had low viscosity enough to infiltrate at 700 °C, infiltration started at that temperature and infiltrated up to 20 μm or so with temperature increase, but infiltration depth did not increase noticeably above 750 °C. Based on these results, when sintered at 900 °C with controlled sheet thickness of both glass and alumina, the shrinkage in *x*–*y* direction was calculated as less than 0.2%, with 40% in *z* direction. Dielectric constant (ε_r) measured 6.19 with quality factor (Q) of 552 at 1 GHz of frequency. From these results, it is thought that zero-shrinkage ceramic substrates would be obtained without de-lamination.

Keywords LTCC · Zero shrinkage · Infiltration · Al_2O_3/glass/Al_2O_3 structure

J.-H. You · D.-H. Yeo (✉) · H.-S. Shin · J.-H. Kim
System Module Team Division of Fusion and Convergence Technology, KICET,
Seoul 153-801, South Korea
e-mail: ydh7@kicet.re.kr

H.-G. Yoon
Division of Materials Science and Engineering, Korea University,
Seoul 133-791, South Korea

1 Introduction

Miniaturization with light weight, multifunctionality and technical fusion of electronic devices and their components are the emerging issues with rapid advance of mobile communication [1]. Along these trends, low temperature cofired ceramic (LTCC) is highly expected for its possibility of embedding-related techniques for high integrity [2]. It is much easier for LTCC to be embedded with passive components than polymer or high temperature cofired ceramic (HTCC) substrates. It is important to ensure dimensional precision and reproducibility of high-frequency properties for high-integrity substrates. For these, need for zero-shrinkage and constrained sintering is increasing [3, 4]. The freely-sintered LTCCs usually have sintering shrinkage between 12% and 16% in the *x*–*y* direction (radial) and slightly more in the thickness (axial) direction. Therefore, pattern misalignment among layers would be occurred.

There have been proposed several zero-shrinkage methods such as pressure assisted method [5], pressure-less assisted method [6], and self-constrained sintering method. It is impossible for pressure assisted method to form precise cavities and difficult to be capable of mass production. There is thickness limitation in multilayer-structure adaptation for pressure-less assisted method and it must be accompanied by removal of constrained layer. And there have been few reports about self-constrained sintering method which was proposed by 'Heraeus' company as 'LTCC/Al_2O_3/LTCC' structure [5–7].

In this study, the shrinkage control in *x*–*y* direction was investigated with fabricating multilayer-structured substrate of 'Al_2O_3/glass/Al_2O_3'. Two kinds of alumina with different particle size (as D_{50} of 0.5 and 1.8 μm) were used to observe glass infiltration behavior. And also, shrinkage in

Table 1 Specifications of raw materials.

Composition	Density (g/cm^3)	Particle size (μm)	T_g (°C)
Al_2O_3 (AES11)	3.93	0.5	–
Al_2O_3 (AES23)	3.77	1.8	–
$ZnO–B_2O_3–PbO–SiO_2$	4.87	2.53	455

x–y, *z* direction, sintered density, crystalline phases, microstructure and dielectric properties were evaluated.

2 Experimental procedure

Commercial powders of alumina (AES-11 (D_{50}=0.5 μm), AES-23 (D_{50}=1.8 μm), Sumitomo Co., Japan) and $ZnO–B_2O_3–PbO–SiO_2$ glass (Phoenix PDE, Korea) were used as raw materials. Used alumina powders are very representative commercial ones for electroceramics. Their specifications are shown in Table 1. Mixtures of each powder with dispersant (SN-9228, SanNopco, Japna), plasticizer (dibutyl phthalate, Daejung Chemical Co., Korea), binder (polyvinyl butylal, BM-SZ, Sekisui, Japan) were ball-milled for 24 h respectively. Prepared slurries were de-gassed and casted into green sheets of uniform thickness. As shown in Fig. 1, casted sheets were fabricated with both alumina (with thickness of 100 and 20 μm) and glass (with thickness of 100 and 30 μm) sheets to have the structure of 'Al_2O_3/glass/Al_2O_3'. Laminated sheets were hot-pressed at 250 bar with warm isostatic press (WIP), followed by cutting into size of 15×15 mm. Cut sheets were fired at 450 °C for binder burn-out and then sintered at 900 °C for 15 min. Glass infiltration depth in the microstructure was observed by field emission scanning electron microscope (JSM-6700F, JEOL, Japan) and *x–y* and *z* direction shrinkage was measured with optical microscope (Icamscope-G, Icamscope, Korea). Sintered density was measured by Archimedean method and crystalline phase was identified by high temperature X-ray diffractometer (D/MAX2500, Mac Sci. Co. Ltd., Japan). Dielectric constants and losses were evaluated at 1 GHz by RF Impedance/Material analyzer (E4991A, 1 MHz–3 GHz, Agilent, USA).

3 Results and discussion

Figure 2 shows glass infiltration depth plots into alumina particle layer of different particle size with temperature variation. Glass infiltration started at 650 °C and showed about 20 μm of maximum value above 750 °C in the case of 0.5 μm-alumina, while 30 μm for 1.8 μm-alumina. Glass infiltration might be estimated by Washburn's relation [8, 9]. It was noted that the time to achieve a given penetration depth could be believed to be directly proportional to the pore radius. Lee et al. [10] reported that infiltration depth would be a function of infiltration time for different particle sizes of alumina powders. In that relation, the infiltration depth is parabolic in time and the penetration rate constant increases with raising the alumina particle size due to the increases of pore size. Figure 2 showed penetration distance of both 0.5 and 1.8 μm-alumina in same condition as similar result as mentioned above.

Figure 3 is patterns of high-temperature X-ray diffractometry with variation of sintering temperature for the substrates of 'Al_2O_3/glass/Al_2O_3' structure using 0.5 μm alumina. There was no phase change up to 750 °C, $PbAl_2Si_2O_8$ phase between alumina and glass was appeared to form rapidly after 800 °C. This result was same for 1.8 μm alumina. Peaks of platinum were thought to be due to testing holder. Figure 4 showed SEM image of substrate sintered at 900 °C after co-laminated with glass and alumina sheet. The image could be divided into three regions of 1 (alumina region), 2 (alumina–glass interfacial region) and 3 (glass region). The qualitative analysis by EDS appeared in Table 2. Zhu et al. [11] reported that glass infiltration was suppressed by formation of crystalline phase between alumina and glass at certain high temperature, though increase of infiltration depth continues till that temperature as glass viscosity decreases. It can be inferred that the most important factors for glass infiltration are the low chemical reactivity with alumina as well as the low viscosity at high temperature.[12]

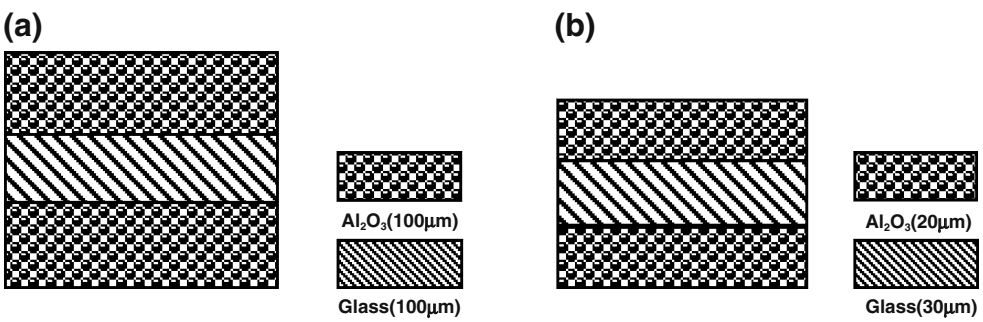

Fig. 1 (**a**) and (**b**) Schematic cross section of laminated green sheets

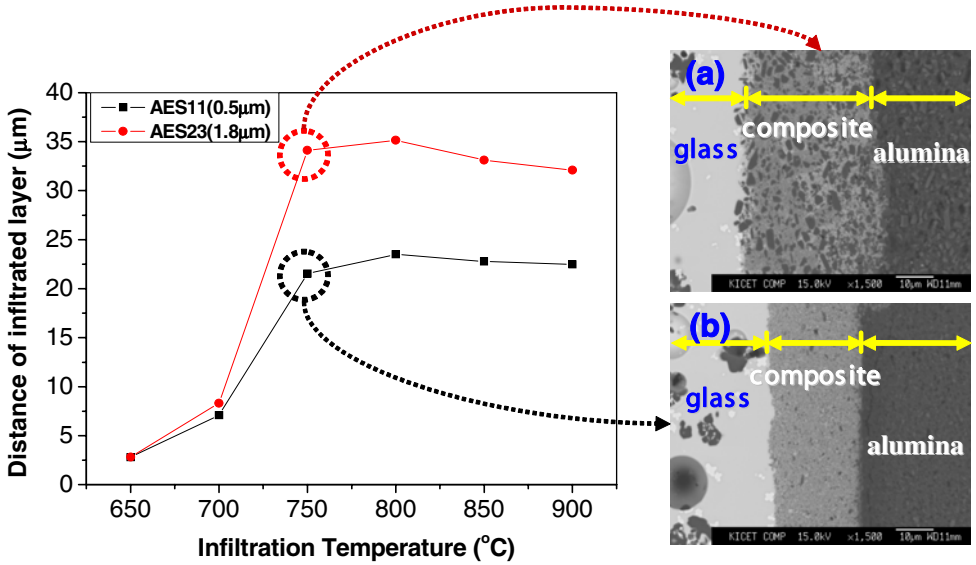

Fig. 2 Distance of glass infiltration in 'Al_2O_3/glass/Al_2O_3' substrates with sintering temperature of 750 °C; (**a**) 1.8 μm, (**b**) 0.5 μm of alumina particle size

Figure 5 shows shrinkage behavior for the substrates of 'Al_2O_3/glass/Al_2O_3' structure using 0.5 μm alumina. Orthogonally cut green sheet of 'Al_2O_3/glass/Al_2O_3' structure was sintered at 900 °C and compared with the rest green sheet in Fig. 5(a). *x*–*y* direction shrinkage was below 0.2%. *z* direction shrinkage increased stiffly up to 800 °C and gradually till 900 °C to the value of 40%, as shown in Fig. 5(b). Sintered density at 900 °C was 3.82 g/cm^3. On the basis of measured porosity, particle packing ratio was calculated as 52% for alumina layer and 44% for glass layer. From these values, relative sintered density was expected as 91% without second phase formation, but it was difficult to calculate precise value due to the second phase formation. Figure 6 for the substrates of 'Al_2O_3/glass/Al_2O_3' structure using 0.5 μm alumina, three bundles were laminated (a) and sintered at 900 °C (c), and their cross-sections were observed with FE-SEM. Bright region was for glass and dark region for alumina. As can be seen in Fig. 6(c), sufficient glass infiltration into alumina layers made substrate fully densified with only 1–2 μm thickness of remained glass layer. Figure 6(b) is magnified section in the alumina layer in (a), where separate alumina particles could be seen and infiltrated glass with isolated alumina particles (dark spots) showed good state of sintering in Fig. 6(d). Though there were remained glass layers un-infiltrated, homogeneous zero-shrinkage substrate would be possible with more precise control of glass layer thickness.

Dielectric constant and quality factor were plotted in Fig. 7 for the substrates of 'Al_2O_3/glass/Al_2O_3' structure using 0.5 μm alumina with variation of sintering temperature. Dielectric constant increased up to 800 °C, then decreased above that temperature. Quality factor simply increased with temperature. According to mixing rule of

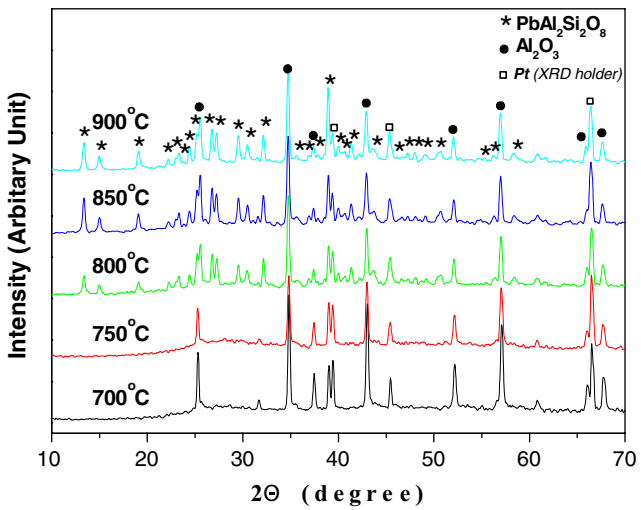

Fig. 3 XRD patterns of Al_2O_3/glass/Al_2O_3 substrates sintered at various temperature

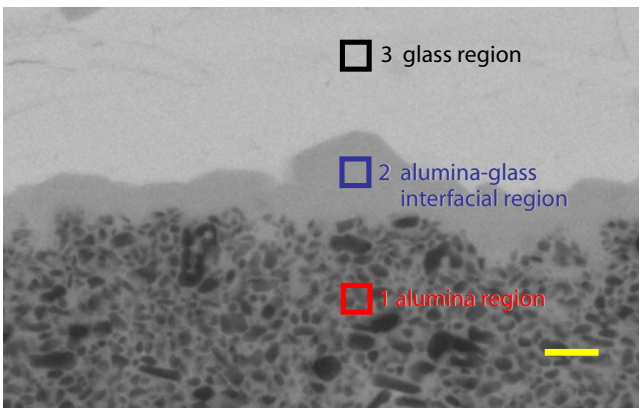

Fig. 4 SEM image of interface of Glass/Al_2O_3 sintered at 900 °C

Table 2 EDS data of interface of glass/Al_2O_3 sintered at 900 °C.

Spectrum	O	Al	Si	Ti	Pb	Total (wt%)
1	53.96	23.69	5.21		17.13	100.00
2	46.02	9.91	10.11		33.96	100.00
3	39.20	3.16	8.67	0.62	48.34	100.00
Max.	53.96	23.69	10.11	0.62	48.34	
Min.	39.20	3.16	5.21	0.00	17.13	

dielectricity [13], it is thought that above 800 °C, dielectric property of each phase in Fig. 4 was responsible for the decreases of dielectric constant and constant increase of quality factor with gradual densification of substrate as temperature increased. It is necessary to determine the dielectric properties among these phases to clarify that of the substrate. Dielectric constant (K) was 6.19 and quality factor (Q) was 552 at 1 GHz and 900 °C.

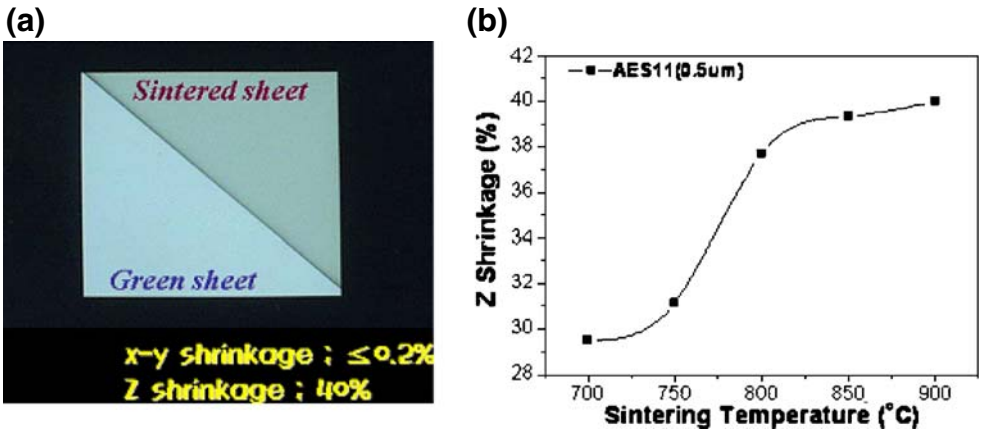

Fig. 5 (**a**) Size comparison of Al_2O_3/glass/Al_2O_3 substrates sintered at 900 °C with green sheet, (**b**) z-direction shrinkage of Al_2O_3/glass/Al_2O_3

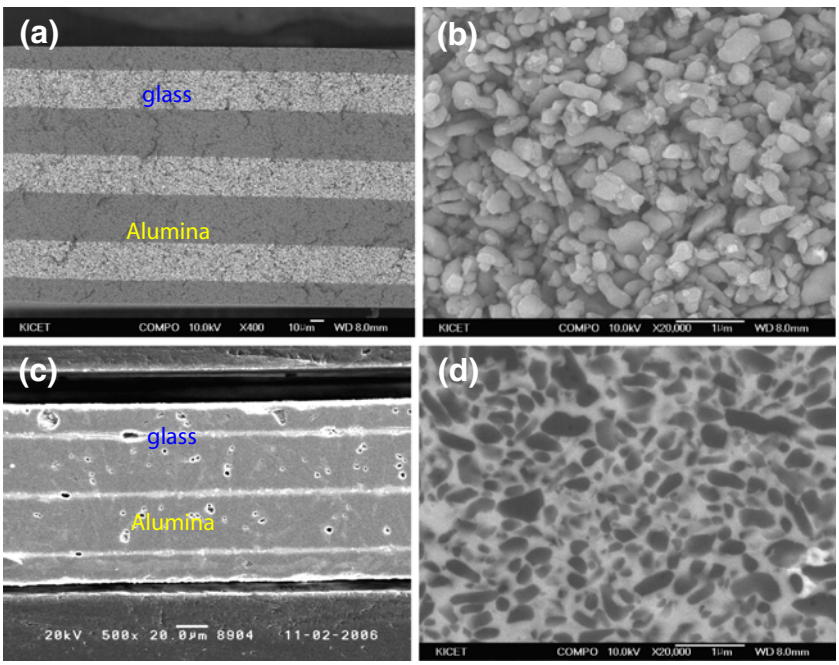

Fig. 6 SEM images of three bundle substrates of Al_2O_3/glass/Al_2O_3 structure; (**a**) three bundle substrate before sintering, (**b**) Al_2O_3 layer before sintering, (**c**) cofired substrate after sintering at 900 °C, (**d**) Al_2O_3 layer after sintering at 900 °C

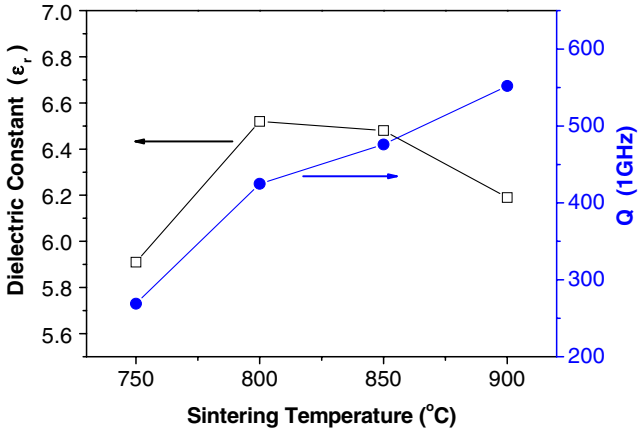

Fig. 7 Dielectric constants and quality factors of Al_2O_3/glass/Al_2O_3 substrates sintered at various temperature

4 Conclusion

In this study, sintering behavior and potential validity as LTCC zero-shrinkage substrate of 'Al_2O_3/glass/Al_2O_3' structure were investigated with use of alumina of different particle size (as D_{50} of 0.5 and 1.8 μm). Full infiltration depth into alumina layer of glass were 20 and 30 μm for D_{50} of 0.5 and 1.8 μm, respectively at 750 °C. Formation of $PbAl_2Si_2O_8$ between alumina and glass above 800 °C was thought to suppress glass infiltration. For 'Al_2O_3/glass/Al_2O_3' structured substrate with use of 0.5 μm-D_{50} alumina sintered at 900 °C, x–y direction shrinkage was below 0.2%, in z direction about 40%. Sintered density was 3.82 g/cm^3 and dielectric constant was 6.19 and quality factor was 552 at 1 GHz.

References

1. R.R. Tummala, J. Am. Ceram. Soc **74**(5), 895–908 (1991)
2. M. Rodriguez, D. Yang, P. Kotula, D. Dimos, J. Electroceram **5**, 217–223 (2000)
3. M. Baker, R. Draudt, in *Proceedings of the 2001 International Symposium on Microelectronic*, pp. 26–31 (2001)
4. M. Hagymasi et al., J. Eur. Ceram. Soc **25**, 2061–2064 (2005)
5. W.A. Vitrio, R.L. Brown, U. S. Patent No. 4656552, (1987)
6. K.R. Mikeska, D.T. Schaefer, U. S. Patent No. 5454741, (1994)
7. F. Lautzenhiser, E. Amaya, Am. Ceram. Soc. Bull **81**, 27–32 (2002)
8. E.O. Einset, J. Am. Ceram. Soc **79**, 333–338 (1996)
9. Y. Pan, X.S. Yi, J. Am. Ceram. Soc. **82**, 3459–3465 (1999)
10. D. Yong Lee et al., Mater. Sci. Eng **A341**, 98–105 (2003)
11. Q. Zhu et al., J. Eur. Ceram. Soc **25**, 633–638 (2005)
12. W.D. Wolf, K.J. Vaida, L.F. Francis, J. Am. Ceram. Soc **79**, 1769–1776 (1996)
13. K. Fukuda, R. Kitoh, I. Awa, Jpn. J. Appl. Phys **32**, 4584–4588 (1993)